Welding in the World
https://doi.org/10.1007/s40194-025-02080-9

RESEARCH PAPER

Multiaxial fatigue life calculation of welded joints made of ductile materials

Niklas Michael Bauer[1] · **Jörg Baumgartner**[1]

Received: 16 December 2024 / Accepted: 18 May 2025

Abstract

Welded joints made of ductile materials exhibit a significant reduction in fatigue life under non-proportional multiaxial loading compared to proportional loading. Different methods to calculate multiaxial fatigue life are evaluated on a comprehensive database, which is created based on various fatigue tests showing ductile material behavior under uniaxial, proportional, and out-of-phase loading. This paper finds that well-known stress-based methods widely used in the literature to evaluate multiaxial fatigue of welded joints cannot accurately calculate fatigue life under both proportional and non-proportional loading for welded ductile materials. Two new methods providing reliable and accurate fatigue life predictions with little scatter under both constant and variable amplitude loading are developed, analyzed in detail, and compared to existing approaches. The new methods include an interaction equation derived from the criteria proposed in codes and standards, as well as a machine learning approach based on artificial neural networks, both developed and optimized or trained based on the created database. Using interpretable machine learning, the neural networks are found to have learned similar correlations between multiaxial loading and fatigue life as those represented by the new interaction equation.

Keywords Fatigue life prediction · Non-proportional loading · Welded joints · Machine learning · Explainable artificial intelligence

Abbreviations

δ	Plane orientation, °
φ	Phase shift, °
σ	Stress component, MPa
$\sigma_\perp$	Stress normal to the weld, MPa
$\sigma_\parallel$	Stress parallel to the weld, MPa
τ	Shear stress, MPa
Δ	Range, -
f_N	Ratio of predicted to experimental fatigue life, -
m	Slope of the S–N curve before the knee point, -
m^*	Slope of the S–N curve after the knee point, -
n	Number of fatigue tests, -
$n_{i/j}$	Number of cycles for given load spectrum block, -
r_{ref}	Reference radius, mm
t	Plate thickness, mm
u	Cyclic degree of utilization, -
CV	Comparison value, -
D_{spec}	Specified Miner sum, -
E	Expected value
$K_{t,\sigma}$	Notch stress concentration factor for normal stress, -
$K_{t,\tau}$	Notch stress concentration factor for shear stress, -
L_s	Spectrum length, -
N	Cycle number, -
$RMSE$	Root mean square error, -
SD	Empirical standard deviation,

Recommended for publication by Commission XIII - Fatigue of Welded Components and Structures.

✉ Niklas Michael Bauer
niklas.michael.bauer@lbf.fraunhofer.de

1 Division Structural Durability, Fraunhofer Institute for Structural Durability and System Reliability LBF, Darmstadt, Germany

1 Introduction

In contrast to semi-ductile and brittle materials, ductile materials and welded joints made of ductile materials show a significant reduction in fatigue life under multiaxial non-proportional loading compared to proportional loading [1, 2]. Non-proportional loading is defined by a varying ratio between two applied stress components over time. However, no comparative study of multiaxial assessment approaches explicitly focusing on ductile material behavior has been conducted for welded joints. In the absence of a uniform definition of when a welded joint can be considered ductile, this paper refers to ductile material behavior, defined as a fatigue life reduction under non-proportional compared to proportional loading. In order to evaluate and analyze approaches that have been applied to evaluate multiaxial fatigue of welded joints in the literature and to develop more reliable and accurate methods, both with respect to ductile material behavior, a comprehensive database is created. The database consists of all publicly available fatigue tests of welded joints which show a fatigue life reduction under out-of-phase loading that the authors could find, including both constant and variable amplitude loading. A new method is derived from the approaches in the literature and optimized with respect to the created database. Furthermore, artificial neural networks are developed and trained on the fatigue data to predict fatigue life. Both the promising approaches from the literature and the newly developed methods are evaluated, analyzed in detail, and compared based on the fatigue data and an interpretable machine learning approach to identify and recommend methods reliably and accurately predicting fatigue life of welded specimens made of ductile materials subjected to proportional and out-of-phase loading.

2 Multiaxial fatigue criteria

Stress-based fatigue life assessment approaches for welded joints generally fall into four categories: equivalent stresses, interaction equations, critical plane approaches, and integral approaches:

- Equivalent stresses are defined as functions of all stress components, with the established ones being invariants which do not depend on the choice of the coordinate system.
- Critical plane approaches define an equivalent stress based on the coordinate plane for which the equivalent stress is highest.
- Interaction equations describe the relationship between different stress components and the fatigue life based on the cyclic degree of utilization of each stress component. Because they are generally easy to use, codes and standards recommend criteria based on interaction equations for fatigue assessment under multiaxial loading [3–5].
- Similar to the critical plane approaches, the integral approaches calculate an equivalent stress for each plane orientation. But instead of selecting the critical plane for the assessment, the equivalent stress is integrated over each plane orientation.

Table 1 provides an overview of the stress-based assessment approaches that have been used for welded joints under multiaxial loading in the literature.

In order to correctly assess the fatigue life of welded joints made from ductile materials under general loading conditions, suitable approaches must consider the reduction in fatigue life due to non-proportional loading. However, both the equivalent stresses and the critical plane approaches based on equivalent stresses, such as the well-known Findley criterion, are in principle not suited to assess ductile materials as they inherently predict higher fatigue life under out-of-phase loading because the equivalent stress is lower when the maxima of the stress components occur at different times, as illustrated in [21]. Furthermore, [1, 2] state that critical plane approaches are suitable for evaluating both brittle and semi-ductile materials, whereas ductile materials should be assessed with an integral of the shear stress over all coordinate planes to correctly incorporate the damage cause, which is done by the effective equivalent stress hypothesis (EESH). Other methods such as the criterion from the Eurocode 3 and the approach by Papadopoulos do not distinguish between proportional and non-proportional loading. Consequently, and with a focus on practical applicability for both constant and variable amplitude loading, i.e., without overly high complexity, dependence on

Table 1 Overview of methods used to assess fatigue life of welded specimens under multiaxial loading

Fatigue life assessment approaches
Equivalent stresses
Principal stress
von Mises
Tresca
DNV [6]
Critical plane approaches
Findley [7]
Matake [8]
Dang Van [9]
McDiarmid [10]
Modified Wöhler Curve Method [11]
Carpinteri-Spagnoli [12]
KoNoS [13]
Interaction equations
Gough-Pollard (IIW-recommendations) [3]
Eurocode 3 [4]
FKM [5]
Integral approaches
Papadopoulos [14]
Effective equivalent stress hypothesis [15]
Shear stress intensity hypothesis [16]
Multiax-Invariant [17]
Others
Stress space curve hypothesis [18–20]

usually unknown material parameters, and an unclear assessment of general stress-time-histories, the Gough-Pollard criterion (GPC), the FKM criterion (FKMC), and the EESH are identified as promising approaches. All the interaction equations and the EESH, all of which are among the most popular criteria used in the literature, are evaluated in the following.

All criteria could be combined with a penalty factor, reducing the fatigue resistance or increasing the effective stress under non-proportional loading, as proposed by the DNV with a penalty factor of 1.1 [6] or implied by the GPC with the comparison value of 0.5 [3]. However, this approach leads to the problem that a constant penalty factor is applied even if one stress component becomes insignificant and the loading tends to become uniaxial, resulting in highly conservative evaluations as the influence of non-proportional loading tends toward zero. Hence, this requires a second criterion to assess whether both stress components are significant enough to apply the penalty factor, which is given by the IIW recommendations, or a penalty factor depending on the amplitudes of both stress components.

2.1 Interaction equations

The fatigue assessment criteria proposed by the IIW [3], the Eurocode 3 [4], or the FKM-guideline [5] are derived from interaction equations which are based on the cyclic degree of utilization u for a given stress component σ:

$$u_\sigma(N) = \frac{\Delta\sigma}{\Delta\sigma_R(N)} \tag{1}$$

where $\Delta\sigma$ denotes the applied stress range and $\Delta\sigma_R$ the endurable stress range derived from the respective resistance S–N curve at a given number of cycles N. All interaction equations represent a curve within two or three dimensions based on the respective stress components for a specific fatigue life. The IIW recommends the use of the ellipsoidal GPC

$$u_{\sigma_\perp}(N)^2 + u_\tau(N)^2 + u_{\sigma_\parallel}(N)^2 \leq CV \tag{2}$$

based on the utilization of the stress normal to the weld $\sigma_\perp$, the shear stress τ, and the stress parallel to the weld $\sigma_\parallel$ with a comparison value CV equal to 1 for proportional loading and 0.5 if the loading is non-proportional, if the shear stress range is greater than 15% of the normal stress range or vice versa, and if the principal stress direction varies by 20° or more. A similar criterion is suggested by the Eurocode 3 (ECC). However, no differentiation is made between proportional and non-proportional loading and the stress component parallel to the weld is neglected:

$$u_{\sigma_\perp}(N)^3 + u_\tau(N)^5 \leq 1. \tag{3}$$

Finally, the FKM-guideline proposes one criterion based on the principal stress for proportional loading:

$$\frac{1}{2}\left(\left|u_{\sigma_\perp}(N) + u_{\sigma_\parallel}(N)\right| + \sqrt{\left(u_{\sigma_\perp}(N) - u_{\sigma_\parallel}(N)\right)^2 + 4u_\tau(N)^2}\right) \leq 1 \tag{4}$$

and another one for non-proportional loading:

$$u_{\sigma_\perp}(N) + u_\tau(N) + u_{\sigma_\parallel}(N) \leq 1. \tag{5}$$

The fatigue life is calculated numerically for each criterion by converting the inequation to an equation which is solved with respect to N. Stresses parallel to the weld resulting from an obstruction of transverse contraction in the weld notch under stress normal to the weld are implicitly accounted for in the resistance S–N curves and do not need to be explicitly calculated; see [22] for a detailed explanation. All criteria describe a super elliptical (two stress components) or super ellipsoidal (three stress components) relationship between the stress components for a given fatigue life.

Variable amplitude loadings can be transformed to equivalent constant amplitude stress ranges according to the Palmgren–Miner rule as suggested by the IIW [3]:

$$\Delta\sigma_{eq} = \sqrt[m_k]{\frac{1}{D_{spec}} \bullet \frac{\sum\left(n_i \bullet \Delta\sigma_i^{m_k}\right) + \Delta\sigma_{knee}^{m_k - m_l} \bullet \sum\left(n_j \bullet \Delta\sigma_j^{m_l}\right)}{\sum n_i + \sum n_j}} \tag{6}$$

with the slope of the reference S–N curve m and the stress ranges $\Delta\sigma$ and corresponding number of cycles n of a specific stress range. The indices i and k refer to the values above the knee point of the S–N curve, while the indices j and l refer to those below the knee point for $\Delta\sigma_{eq} \geq \Delta\sigma_{knee}$ and vice versa in case of $\Delta\sigma_{eq} < \Delta\sigma_{knee}$. The specified Miner sum D_{spec} equals 0.5 assuming no high fluctuations of mean stresses [23].

2.2 Effective equivalent stress hypothesis

The EESH [15] assumes that the shortened fatigue life under non-proportional loading results from dislocations caused by the interaction of shear stresses in different coordinate plane orientations. Hence, a damage parameter $F(\varphi)$ is introduced as the integral of the shear stress τ over all plane orientations δ orthogonal to the surface for a given phase shift φ between normal and shear stress. The damage parameter is calculated based on local stresses as follows:

$$F(\varphi) = \frac{1}{\pi}\int_0^\pi f_p(\varphi, \delta)d\delta \tag{7}$$

with

$$f_p(\varphi, \delta) = \tau(\varphi, \delta) \tag{8}$$

for constant amplitude loading and

$$f_p(\varphi,\delta) = \frac{1}{L_s}\sum_{i=1}^{L_s}\tau_i(\varphi,\delta) \tag{9}$$

for variable amplitude loading, where L_s denotes the spectrum length [24]. The effective equivalent stress is defined for proportional loading as a modification of the von Mises stress with the size factor f_s:

$$\sigma_{EESH}(\varphi = 0°) = \sqrt{\sigma_x^2 + \sigma_y^2 - \sigma_x\sigma_y + f_s^2 \bullet 3\tau_{xy}^2} \tag{10}$$

$$f_s = \sqrt{\frac{\sigma_x^2 + \sigma_y^2 - \sigma_x\sigma_y}{3\tau_{xy}^2}}. \tag{11}$$

The stress component parallel to the weld resulting from an obstruction of transverse contraction is again implicitly accounted for in the resistance S–N curves and does not need to be explicitly considered. Out-of-phase loading can be assessed using a non-proportionality factor which leads to the final formulation of the effective equivalent stress:

$$\sigma_{EESH}(\varphi) = \sigma_{EESH}(\varphi = 0°)\frac{F(\varphi)}{F(\varphi = 0°)} \bullet \sqrt{S^z} \tag{12}$$

with

$$S = \frac{1 + K_{t,\sigma}}{1 + K_{t,\tau}}, z = 1 - \left(\frac{\varphi - 90°}{90°}\right)^2 \tag{13}$$

and the effective notch stress concentration factors for normal stress $K_{t,\sigma}$ and shear stress $K_{t,\tau}$, which could also be substituted by the normalized stress gradients. Finally, the effective equivalent stress is evaluated against the S–N curve for stress normal to the weld.

The size factor f_s assumes equal slopes of the S–N curves for normal and shear stress. The introduction of a fatigue life dependent size factor as proposed in [25] allows for the consideration of different slopes:

$$f_s = \sqrt{\frac{\sigma_x^2\left(N\left(\tau_{xy}\right)\right) + \sigma_y^2\left(N\left(\tau_{xy}\right)\right) - \sigma_x\left(N\left(\tau_{xy}\right)\right)\sigma_y\left(N\left(\tau_{xy}\right)\right)}{3\tau_{xy}^2}} \tag{14}$$

where the normal stress components are derived from the corresponding S–N curves at the cycle number N which is again derived from the shear stress S–N curve at the applied shear stress.

3 Methodology

In order to evaluate and compare fatigue assessment approaches, a comprehensive database is created containing fatigue tests of welded joints under uniaxial, proportional, and out-of-phase loading exhibiting ductile material behavior, including constant and variable amplitudes. Since all interaction equations for non-proportional loading are based on the general equation of a super ellipse considering the stress normal to the weld and the shear stress, a new super ellipse criterion (SEC) is developed by optimizing the parameter of the super ellipse equation with respect to the present database. Furthermore, artificial neural networks (NN) are developed and trained based on the present database to predict fatigue life. The interaction equations, including the GPC, the FKMC, the ECC, and the SEC, the EESH, and the NN are evaluated and compared by predicting fatigue life based on the created database. All evaluations are based on nominal stresses. Finally, both the interaction equations and the NN are interpreted, analyzed, and evaluated with respect to the underlying relationship between fatigue life and applied stress.

3.1 Database

The database consists of all fatigue tests of welded joints under out-of-phase loading due to stresses normal to the weld and shear stresses while showing ductile material behavior that the authors could find, plus the corresponding uniaxial and proportional fatigue tests. Non-proportional loads other than out-of-phase are not part of this paper because of the limited number of fatigue tests available in the literature. The stress component parallel to the weld is not applied in combination with shear stresses and non-proportional loading in any of the known experiments and is therefore not further considered. Data is excluded if the required uniaxial reference S–N curves for normal and shear stresses could not be derived from the experiments due to insufficient fatigue tests or if the loading exhibits non-proportionality other than phase shifts. A few individual fatigue tests from the experiments by Wiebesiek [25] showing brittle material behavior at low load levels are also excluded. Thus, the database contains 437 multiaxial fatigue tests, excluding runouts, from 14 test programs, which are outlined in Table 2 and Fig. 1.

Variable amplitude loading always refers to Gaussian distributions and the failure criteria were through-thickness cracking or fracture. Other publications containing fatigue test data of welded specimens under multiaxial loading are not relevant due to non-ductile material behavior [35–38], which is defined as increasing or equal fatigue life under non-proportional loading compared to proportional loading, insufficient data to derive all uniaxial S–N curves [39–42], multiaxial loading other than out-of-phase loading [43–50], or only normal stress components [51].

3.2 Fatigue life calculation

All methods presented in this paper rely on the applied load and the respective uniaxial fatigue resistance S–N curves

Table 2 Multiaxial fatigue database for welded joints under ductile material behavior and out-of-phase loading (*T-T*: tube-tube, *T-F*: tube-flange, *aw*: as welded, *sr*: stress relieved, *gr*: ground flush, *P*: proportional, *OOP*: out-of-phase, *specimens from Razmjoo under pure torsion loading partially failed in the weld throat)

#	Primary author(s)	Specimen	Material	Thickness in mm	Post treatment	Amplitude	*R*	Phase shift in °	Failure location	Number P/OOP
01	Eibl [26]	T-T	Steel (St 35)	2	aw	Constant	− 1	90	Root	18/8
02	Exel [27]/Bolchoun [17]	T-T	Magnesium (AZ31)	1.5	aw	Constant/variable	− 1	45, 90/45	Root	18/19
03	Exel [27]/Bolchoun [17]	T-T	Magnesium (AZ61)	1.5	aw	Constant/variable	− 1	45, 90/45	Root	17/22
04	Bertini [28], Frendo [29]	T-F	Steel (S355 JR)	10	aw	Constant	− 1	90	Root	10/9
05	Bertini [28], Frendo [29]	T-F	Steel (S355 JR)	10	aw	Constant	0	90	Root	11/8
06	Razmjoo [30]	T-F	Steel (BS 4360 Grade 50E)	3.2	aw	Constant	0	90	Toe*	7/7
07	Sonsino [31]/Sonsino [32]	T-F	Steel (StE 460)	10	sr	Constant/variable	− 1	90	Toe	15/17
08	Sonsino [31]	T-T	Steel (StE 460)	6	sr + gf	Constant	− 1	90	Toe	9/9
09	Störzel [18]	T-T	Steel (S235 G2 T)	1	aw	Constant	− 1	45, 90	Root	21/24
10	Wiebesiek [25]	T-T	Aluminum (AlMg3,5Mn)	1.5	aw	Constant, variable	− 1	45, 90	Root	27/31
11	Wiebesiek [25]	T-T	Aluminum (AlSi1MgMn T6)	1.5	aw	Constant, variable	− 1	45, 90	Root	23/19
12	Winther [33]	T-T	Steel (S355 J2H)	3.1	aw	Constant	− 1	22.5, 45, 67.5, 90	Toe	5/25
13	Witt [34]	T-F	Steel (StE 460)	8.0	sr	Constant, variable	− 1	90	Toe	16/14
14	Witt [34]	T-F	Steel (StE 460)	8.0	sr	Constant, variable	0	90	Toe	13/15

Fig. 1 Specimens from the database (*specimens differ in sheet thickness)

for the stress normal to the weld and the shear stress. The bilinear S–N curves are statistically derived directly from the corresponding experiments, including the runouts, using the maximum likelihood method while minimizing the scatter in the direction of the fatigue life [52]. Clamping failure is interpreted as a runout. The knee point is assumed at 10^7 cycles for normal stress and 10^8 cycles for shear stress if no knee point can be identified, while the slope after the knee point is assumed to equal 22 according to [3]. The S–N curve parameters are given in Table 8 in Appendix 1. Variable amplitude loading is evaluated by

Table 3 Notch stress concentration factors (*stress concentration factors derived from a fictitious notch radius of 0.05 mm)

Primary author(s)	$K_{t,\sigma}$	$K_{t,\tau}$
Eibl	13.72*	5.89*
Exel, Bolchoun, Wiebesiek	9.95*	4.03*
Bertini, Frendo	2.99	2.60
Razmjoo	5.59*	2.02*
Sonsino (tube-flange)	2.78	1.63
Sonsino (tube-tube)	1.00	1.00
Störzel	9.62*	4.21*
Winther	4.10*	2.28*
Witt	2.99	1.68

deriving constant amplitude equivalents according to Eq. (6), which yields good results consistent with the evaluation of constant amplitudes and ensures comparability. Since both the applied loads and the fatigue resistance are derived directly from the experiments, the chosen stress concept has no effect on the fatigue life calculated by the interaction equations.

Only the EESH is defined specifically for a local stress concept. Therefore, finite element models are generated and meshed according to [53] to derive the notch stress concentration factors K_t, which are presented in Table 3, for each specimen and each stress component. The fictitious notch radius is chosen based on the plate thickness with $r_{\mathrm{ref}} = 0.05\mathrm{mm}$ for a plate thickness $t < 5\mathrm{mm}$ and $r_{\mathrm{ref}} = 1\mathrm{mm}$ otherwise according to [24].

The EESH can be applied based on the original size factor (Eq. (11)) or the modified, fatigue life dependent size factor (Eq. (14)). The root term in Eq. (12) is introduced to account for the effect of the highly stressed material volume on the effective equivalent stress [31] and is only recommended for thick plates with low stress concentrations [54]. In order to determine when to apply the root term and the fatigue life dependent size factor, the EESH is evaluated for each individual test program with and without both the root term and fatigue life dependent size factor based on the root mean square error. The root mean square error *RMSE* is calculated between the logarithmic predicted fatigue life N_{pred} and experimental fatigue life N_{exp}, while being converted to a scalar value for better comprehension:

$$RMSE = 10^{\sqrt{\frac{\sum_{i=1}^{n}\left(\log(N_{exp,i})-\log(N_{pred,i})\right)^2}{n}}} \tag{15}$$

with n being the number of fatigue tests. While the *RMSE* on the basis of logarithmic values represents a difference between logarithmic values, the converted error describes a deviation factor with respect to scalar values. Runouts and variable amplitude loading are excluded. The best configuration is selected for further fatigue life calculation.

3.3 Optimization of the interaction equations

The difference between all interaction equations for non-proportional loading lies in the exponents m, n, and o, the comparison value CV, and the stress components ($\sigma_\perp$, $\sigma_\parallel$, and τ) considered:

$$\left(\frac{\Delta\sigma_\perp}{\Delta\sigma_{\perp_R}(N)}\right)^m + \left(\frac{\Delta\sigma_\parallel}{\Delta\sigma_{\parallel_R}(N)}\right)^n + \left(\frac{\Delta\tau}{\Delta\tau_R(N)}\right)^o \leq CV \quad (16)$$

The super ellipse criterion is developed by empirically optimizing the parameters based on the present database. Since the database does not contain stresses parallel to the weld, this stress component will not be considered further, reducing the ellipsoidal correlation to an elliptical correlation.

The reduction of the comparison value under non-proportional loading, as proposed by the GPC, is equivalent to introducing a penalty factor applied to both stress components. As described in Sect. 2, this leads to problems when assessing non-proportional loading with a dominant stress component. Accordingly, the IIW-recommendations give a percentage of 15% ($\sigma_\perp \leq 0.15 \cdot \tau$ resp. $\tau \leq 0.15 \cdot \sigma_\perp$) under which the influence of non-proportionality can be neglected for the GPC. This leads to a sudden jump in the endurable degree of utilization that is not physically explainable or experimentally justified but necessary, because at least for pure uniaxial loading, a degree of utilization and thus a comparison value of 1 must be applied, since uniaxial loading cannot be non-proportional. In order to improve the assessment and to achieve a consistent evaluation for stress components tending towards zero without the described discontinuity resulting from a variation of the comparison value, the following approach was used. For proportional loading, the exponents are assumed to be equal ($m = n = o$) and optimized based on all proportionally loaded constant amplitude fatigue tests with a comparison value of $CV = 1$. Non-proportionality is considered by adjusting the exponents of both stress components, again assumed to be equal, while keeping a constant comparison value of $CV = 1$. Thus, the reduction in fatigue life due to non-proportional loading increases as the utilizations of both stress components become more similar, while the effect of non-proportionality decreases with a ratio between shear stress and normal stress tending to zero or infinity until no fatigue life reduction is implied under uniaxial loading. Hence, this approach resolves the issue with a constant penalty factor as the changed exponents can be interpreted as a variable penalty factor depending on the ratio between normal and shear stress. The implications of varying the comparison value or the exponents of the super ellipse equation will be illustrated in Sect. 4.4. The exponents for non-proportional loading are derived similarly to those for proportional loading for all constant amplitude out-of-phase fatigue tests. Each optimization is performed individually for each test program and then averaged to give equal weight to each test program. A test program is defined by all fatigue tests associated with the same uniaxial resistance S–N curves for both stress components. Variable amplitudes are not considered to avoid any effect from the transformation to constant amplitude equivalents and runouts are not considered to reduce scatter. The optimization is based on the root mean square error according to Eq. (15).

3.4 Neural networks

Deep NN are trained on constant amplitude fatigue tests including runouts to predict fatigue life for uniaxial, proportional, and out-of-phase loading. The input variables are associated with either the applied load or the fatigue resistance of each stress component against uniaxial loading, which is characterized by the S–N curve parameters derived according to Sect. 3.2, and presented in Table 4. In the case of a proportional load, the phase shift becomes zero. All variables related to fatigue resistance remain the same for each fatigue test within the same test program, even for uniaxial loading. However, the slopes after the knee point for normal and shear stress are highly correlated as they rarely deviate from 22, while being poorly statistically supported and less relevant for evaluating fatigue life in the high cycle fatigue regime. To facilitate and improve the training of the NN, the slope after the knee point based on shear stress is neglected as an input variable. The output variable is the fatigue life.

The NN are trained via supervised learning using mini-batch gradient descent with a ReLU activation function. Due to the limited data and for comparison reasons, training and prediction are based on k-fold cross-validation with k different test programs and one neural network for each test program. This means that the fatigue life of each fatigue test within a test program is calculated by a specific neural network that has been trained on all data except the test program for which

Table 4 Input variables for the neural networks

Symbol	Description
Loading	
$\Delta\sigma_\perp$	Normal stress range
$\triangle\tau$	Shear stress range
φ	Phase shift
Fatigue resistance	
$\Delta\sigma_{\perp,knee}$	Stress range at the knee point (normal stress)
$N_{\sigma_\perp,knee}$	Cycle number at the knee point (normal stress)
$m_{\sigma_\perp}$	Slope before the knee point (normal stress)
$m^*_{\sigma_\perp}$	Slope after the knee point (normal stress)
$\Delta\tau_{knee}$	Stress range at the knee point (shear stress)
$N_{\tau,knee}$	Cycle number at the knee point (shear stress)
m_τ	Slope before the knee point (shear stress)

the fatigue life is being predicted. Hence, similarities between training and prediction data can be avoided.

Training a neural network is generally not a straightforward process, and the success depends heavily on the data used for training, the configuration of the neural network, and the training parameters. All presented input variables must be scaled to similar means and variances. This is achieved using batch normalization after transforming cycle numbers and stresses to logarithmic values. Different and random weight initializations are used to broaden the parameter search landscape, while local minima are avoided using mini-batches and gradient descent with momentum. The risk of overfitting is addressed with dropout and regularization, while the NN performed better without dropout. The loss function is defined as the mean square error of the logarithmic predicted and experimental fatigue life plus the regularization term. Relevant parameters are presented in Table 5.

3.5 Empirical analysis and interpretable machine learning

All interaction equations represent curves depending on the utilization of both stress components. These curves are plotted along with the actual utilizations calculated for each fatigue test under constant amplitude loading from the present database, except the runouts, to analyze how well each curve represents the data. The utilizations are calculated for both stress components based on the applied loads and the fatigue resistances derived from the experimental uniaxial S–N curves at the experimental fatigue life. To reduce scatter, all data points within a test set, which is defined as the same normal to shear stress ratio within a test program, are averaged within the plot. Since the SEC is optimized based on a subset of the data, a superior fit and higher prediction accuracy than any other interaction equation is implied.

To better understand, analyze, and compare the NN with other approaches and to derive possible effects and relationships between the input variables and the fatigue life, the partial dependence plot, a common interpretable machine learning approach, is applied. This is done for each neural network by calculating the predicted fatigue life over various combinations of load-related input variables while keeping the fatigue resistance variables of the corresponding test program constant. All predictions for a given combination of variables are then averaged to derive a partial dependence plot independent of the current test program. Correlations of input variables do not need to be considered due to the nature of the variables.

Table 5 Training parameters for the neural networks

Parameters	Value
Hidden layers	2
Nodes per layer	8
Mini-batch size	10
Momentum	0.5
Dropout	0.0
Regularization	0.5

4 Results

The EESH is evaluated and modified based on different configurations, as described in Sect. 3.2, and the best configuration is derived for further assessment. The parameters from the optimization of the interaction equations are presented and the resulting SEC is introduced. All interaction equations outlined in Sect. 2.1 are evaluated together with the SEC, the modified EESH, and the newly developed NN. Both the interaction equations and the NN are further analyzed and compared in detail.

4.1 Modification of the effective equivalent stress hypothesis

The fatigue life is calculated by the EESH for each test program with and without the consideration of the root term from Eq. (12) and the fatigue life dependent modification of the size factor as described in Eq. (14). The corresponding converted root mean square errors from Eq. (15) are shown in Table 6 for each test program. As the root term is proposed to account for a higher plate thickness, the thickness is listed as well.

Table 6 clearly shows how the fatigue life dependent size factor gives significantly lower prediction errors than the original formulation with and without consideration of the root term. The application of the root term generally shows lower prediction errors for thicker plates and higher prediction errors for thinner plates. Accordingly, the EESH is used for further calculations based on the fatigue life dependent size factor while the root term is applied for plates with $t > 3$mm.

4.2 The super ellipse criterion

As described in Sect. 3.3, the exponents from the interaction equations are optimized separately for each test program to avoid any influence of the sample size of different test programs. All exponents for both fatigue tests under proportional and out-of-phase loading are listed in Table 7, and each exponent applies to both normal and shear stress utilization.

Accordingly, the SEC is defined as follows:

$$\left(\frac{\Delta\sigma_{\perp}}{\Delta\sigma_{\perp_R}(N)}\right)^c + \left(\frac{\Delta\tau}{\Delta\tau_R(N)}\right)^c \leq 1 \tag{17}$$

with $c = 2.15$ for proportional and $c = 1.26$ for non-proportional loading. The individual exponents show moderate

Table 6 Root mean square errors of fatigue life calculation by different configurations of the EESH (*sf(N)*: fatigue life dependent size factor, *rt*: root term)

Test program (plate thickness in mm)	Original	− rt	+ sf(N)	− rt + sf(N)
01 (2.0)	7.68	3.47	3.36	1.80
02 (1.5)	3.87	2.49	2.79	2.95
03 (1.5)	4.55	2.30	3.21	1.88
04 (10.0)	7.39	9.94	2.03	2.30
05 (10.0)	2.81	2.77	1.55	1.63
06 (3.2)	3.06	3.32	1.86	2.63
07 (10.0)	2.29	1.93	2.05	3.21
08 (6.0)	2.80	2.80	2.71	2.71
09 (1.0)	5.48	2.94	2.31	2.43
10 (1.5)	2.67	2.48	1.81	2.13
11 (1.5)	3.59	2.04	2.50	1.52
12 (3.1)	1.82	2.59	1.44	1.96
13 (8.0)	2.39	2.67	2.21	3.04
14 (8.0)	2.91	1.79	2.45	1.80
Average	3.81	3.11	2.31	2.28

Table 7 Optimized exponents of a general interaction equation—same results for $\varphi = 90°$ or $\varphi > 0°$

Test program	Proportional	Out-of-phase
01	2.5	1.6
02	2.0	1.3
03	1.7	1.2
04	1.8	1.0
05	1.8	1.1
06	2.0	1.0
07	1.7	1.0
08	2.3	1.3
09	2.5	1.3
10	2.6	1.1
11	2.7	1.6
12	1.8	1.4
13	2.9	1.2
14	1.8	1.6
Average	2.15	1.26
Empirical standard deviation	0.42	0.22

scatter under proportional loading and low scatter under out-of-phase loading. The differences in scatter are due to the nature of the elliptical equation, as the marginal effect on the curvature of the ellipse decreases with higher exponents. Accordingly, the lower scatter under out-of-phase loading, where exponents are close to one, is expected.

4.3 Fatigue life calculation

Fatigue life N_{pred} is predicted for all fatigue tests under multiaxial loading, including constant and variable amplitudes and excluding runouts, and presented in Fig. 2 over the corresponding experimental fatigue life N_{exp} for each assessment approach. Each phase shift is marked individually. The corresponding logarithmic prediction factors

$$\log(f_N) = \log\left(\frac{N_{\mathrm{pred}}}{N_{\mathrm{exp}}}\right) \tag{18}$$

are calculated for each fatigue tests along with the corresponding expected value E, the empirical standard deviation SD, the root mean square error $RMSE$, and the number of predictions n, while both prediction factors and statistical measures are converted to scalar values for better understanding, similar to the $RMSE$ presented in Eq. (15). Accordingly, an expected value of one represents an accurate prediction as the predicted fatigue life equals the experimental fatigue life. The standard deviation can be interpreted as a factor describing the scatter of the fatigue life prediction factors, with a low standard deviation corresponding to high precision. Similar to the standard deviation, the root mean square error represents a factor describing the deviation from the optimal prediction. The distribution of all fatigue life prediction factors is shown in Fig. 3 on a logarithmic scale together with the corresponding statistical measures.

The criteria proposed in codes and standards, including the ECC, the GPC, and the FKMC, all prove to be incapable of accurately predicting the fatigue life under both proportional and out-of-phase loading. Since the ECC does not distinguish between proportional and non-proportional loading, the overly high predictions under out-of-phase loading and the high scatter are expected. However, the proportional fatigue tests also prove to be non-conservative on average. The FKMC is prone to conservative calculations for both proportional and out-of-phase loading while maintaining a similar expected fatigue life prediction factor with a small standard deviation. While the GPC shows accurate calculations under proportional loading, the comparison value of 0.5 for non-proportional loading results in conservative predictions, as stated in the IIW-recommendations. The SEC from this paper is the only interaction equation that can accurately and precisely predict fatigue life under both proportional and out-of-phase loading with an expected fatigue life prediction factor close to one and the lowest scatter. Assuming a normal distribution, the RMSE of 2.11 means that approximately 68% of all predictions deviate from an optimal prediction by a factor of no more than 2.11. The EESH, modified according to Sect. 4.1, overpredicts fatigue life primarily for out-of-phase loading, while showing moderate scatter. Finally, the NN show the best prediction quality with a mean prediction ratio very close to one and the smallest standard deviation and root mean square error of 1.90.

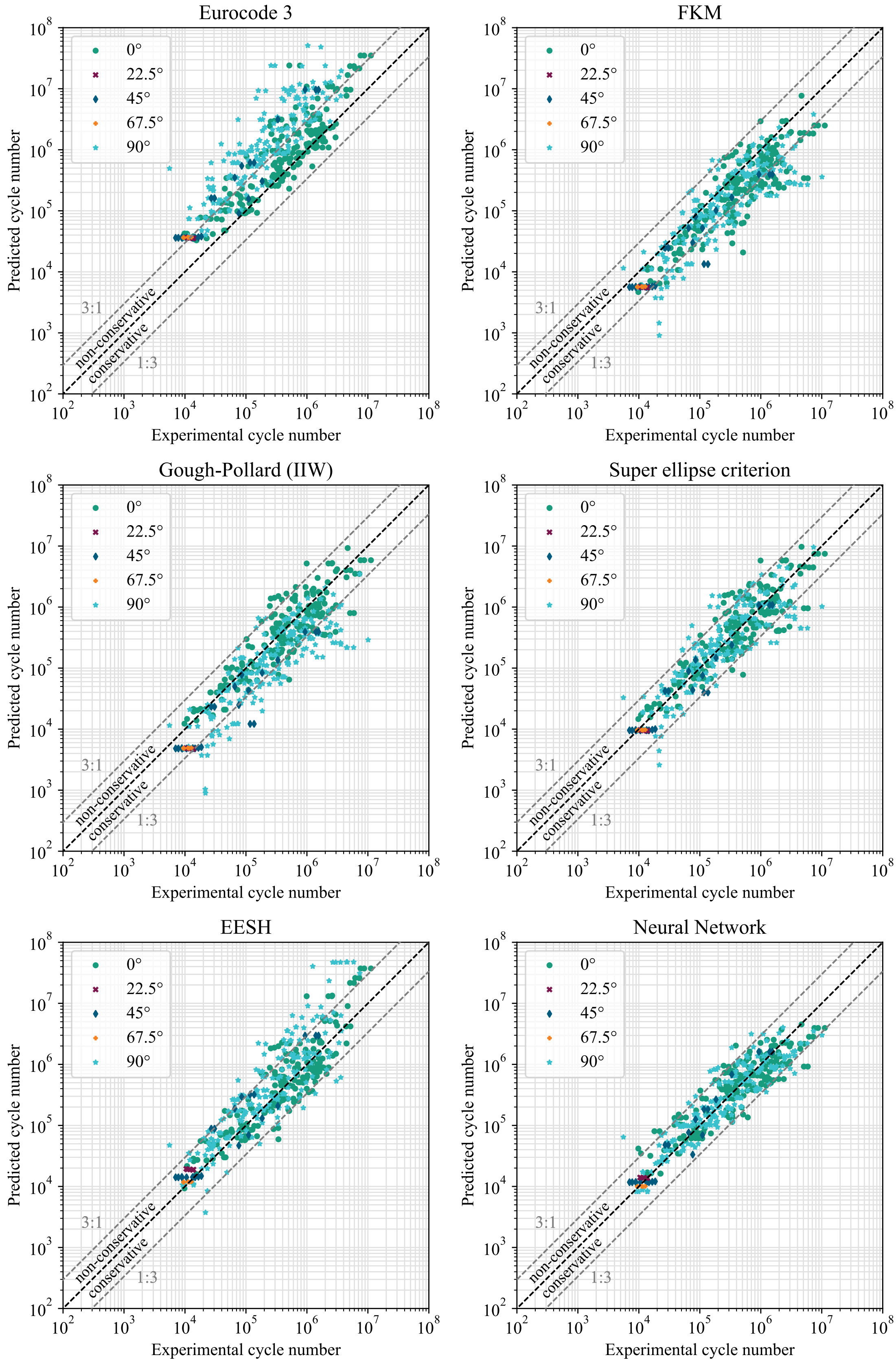

Fig. 2 Fatigue life prediction of welded joints under multiaxial loading for different phase shifts (exemplary fatigue life prediction factors in grey)

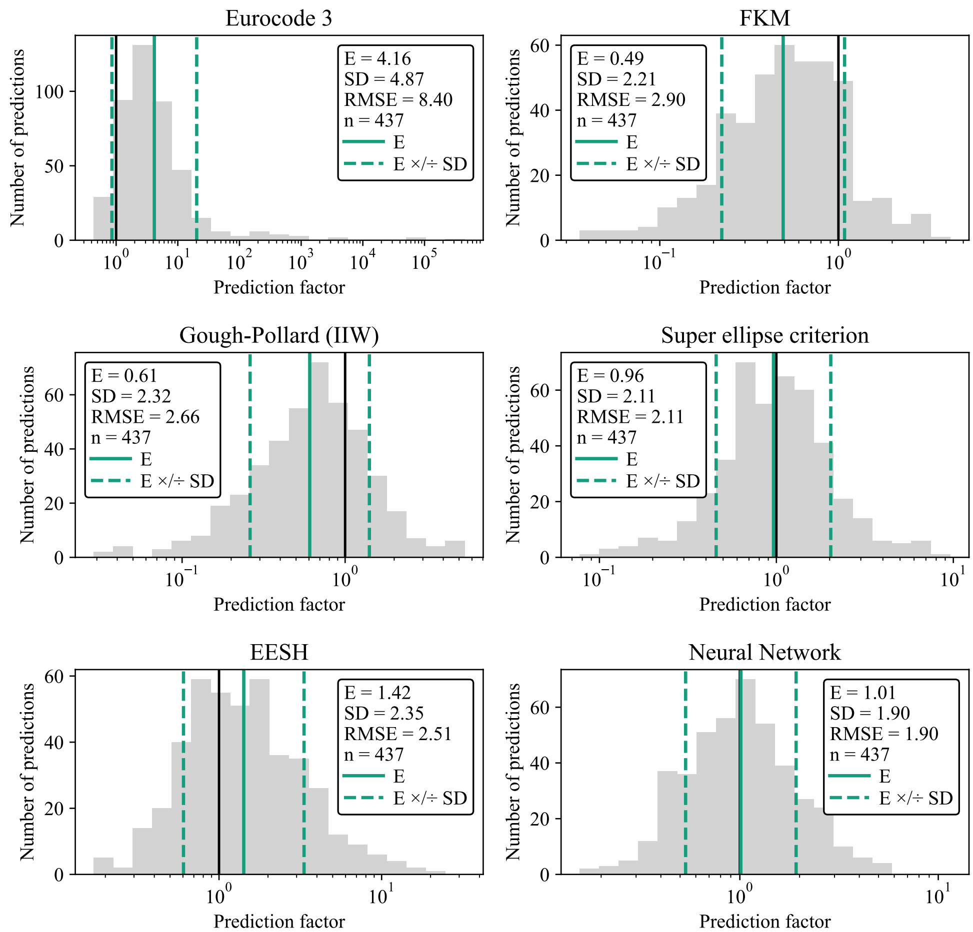

Fig. 3 Ratio of predicted fatigue life to experimental fatigue life under multiaxial loading calculated by different approaches

In order to exclude any possible effects due to the conversion from variable amplitudes to constant amplitude equivalents, the results from Fig. 2 and Fig. 3 are presented for constant amplitude loading only in Appendix 2 in Figures 7 and 8. Nevertheless, both evaluations show very similar results, confirming that the SEC and the NN, which perform equally well under constant amplitude loading, can predict fatigue life for both constant and variable amplitude loading accurately and more precisely than the methods from the literature. Moreover, under constant amplitude loading, the scatter is significantly reduced for all criteria, and the EESH shows only slightly non-conservative results for out-of-phase loading. An explicit differentiation between constant and variable amplitudes and proportional and out-of-phase loading is presented for the SEC in Appendix 3 in Figures 9 and 10, showing that constant amplitude and proportional loads are evaluated better than variable amplitude and out-of-phase loads.

4.4 Detailed analysis and comparison of interaction equations

Figure 4 shows the averaged degrees of utilizations of each test set under constant amplitude uniaxial and proportional loading (top) and out-of-phase loading (bottom) together with the curve from each interaction equation.

Test sets under out-of-phase loading exhibit significantly lower utilizations of both stress components, underlining the fatigue life reducing effect of non-proportional loading, while showing comparable scatter. The findings from Figs. 2 and 3 can be explained by the fit between the degrees of utilization and the respective interaction equation curves. Accordingly, the ECC and the FKMC show significant deviations between the interaction equation curves and the data, while the GPC exhibits a good fit only for proportional loading. The actual correlations between the utilization of both stress components for each test set under uniaxial and proportional loading as well as non-proportional loading are well represented by the super ellipse derived from the SEC.

Since the adjusted comparison value implies a reduction in fatigue life even if one stress component is insignificant (see Sect. 3.3), resulting in an intercept of less than one, the IIW advises against correcting the comparison value in this scenario. The corresponding section is marked exemplary as a dash-dotted line. The curves from both the SEC and the FKMC illustrate the effect of reducing the exponents instead of the comparison value, showing an increasing curvature as the

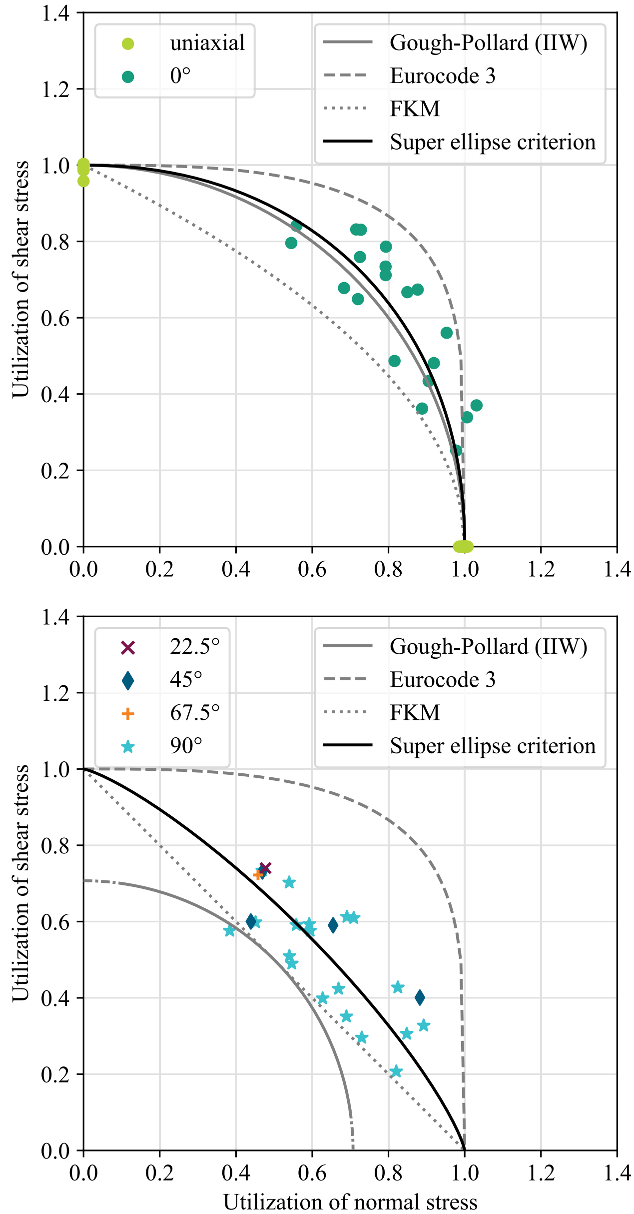

Fig. 4 Cyclic degrees of utilization and curves from interaction equations

exponents increase, while maintaining the necessary intercept of one for both utilizations. Accordingly, fatigue life under non-proportional loading is evaluated similarly to proportional loading when one stress component is insignificant and decreases continuously compared to proportional loading as both utilizations become more similar. In the absence of data from fatigue tests under multiaxial loading where the utilization of one stress component is closer to zero, all criteria can be evaluated only for similar utilizations. However, all curves must end in a utilization of one with one stress component being zero.

Fatigue tests under out-of-phase loading are usually performed with a phase shift of 90°, which is widely assumed to be the most damaging. The few fatigue tests with phase shifts less than 90° are not sufficient to derive a statement about the effect of different phase shifts on fatigue life. Nevertheless, in accordance with [33], there are no obvious differences between phase shifts of 90° and less.

4.5 Interpretation of the neural networks

The NN are interpreted using an averaged partial dependence plot as described in Sect. 3.5. While normal and shear stress are varied, the phase shift is set to zero. The partial dependence plot is shown in Fig. 5 on a logarithmic scale of fatigue life. Equal cycle numbers of different stress combinations are highlighted via isolines. In contrast to the interaction equations, different load levels do not show the exact same relationship between load and fatigue life for a given cycle number. Hence, Fig. 5 is not based on the utilization, but directly on the stress components.

The NN clearly learned super elliptical correlations between normal and shear stress under uniaxial and proportional loading for any given cycle number. The isolines consistently resemble the curves derived from the interaction equations for different cycle numbers, showing no influence of different stress levels on the shape. A variation of stress components shows similar variations in logarithmic fatigue life for all stress levels, representing a linear relationship between logarithmic fatigue life and stress as in the S–N curves. Other effects or dependencies cannot be identified. The increase in fatigue life following an increase of any stress component, especially at high load levels, is caused by missing data in the region of a dominant stress component, as can be seen in Fig. 4.

Interpreting the NN with respect to out-of-phase loading is more complicated because the out-of-phase fatigue tests all show similar degrees of utilization. Hence, selected isolines from Fig. 5 are compared to the corresponding isolines based on a 90° phase shift and presented in Fig. 6 for an area without large differences between both stress components. Smaller phase shifts are not considered due to insufficient data. To compare the NN with the interaction equations with respect to both proportional loading and the effect of out-of-phase loading, the corresponding isolines from the SEC are shown for proportional and out-of-phase loading, while the curves for proportional loading are based on the same uniaxial fatigue resistance as implied by the NN.

Figure 6 shows how similar the isolines from the NN are to those from the SEC, explaining the similar prediction quality. The damaging effect of a phase shift of 90° is comparable in both models. Hence, the NN confirms the super elliptical relationship between stress components or utilizations for the given input variables, while other, more complex correlations could have been learned since the NN has a significantly higher number of degrees of freedom.

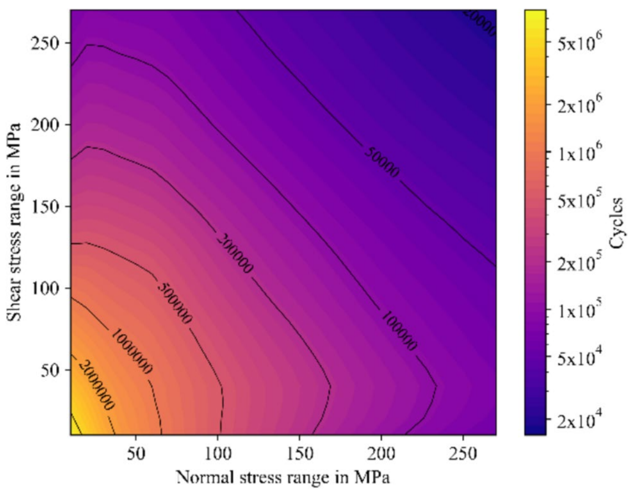

Fig. 5 Partial dependence plot—averaged fatigue life prediction of neural networks under proportional loading

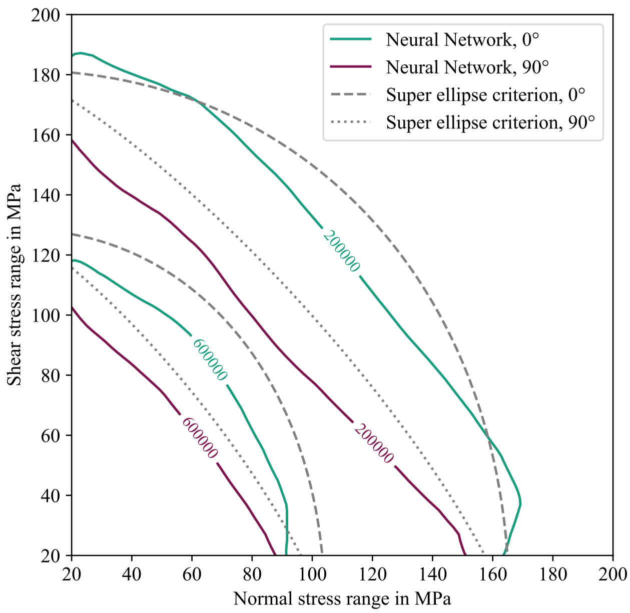

Fig. 6 Isolines of same fatigue life from partial dependence plot and interaction equations for different phase shifts

5 Discussion and outlook

The fatigue life of welded joints made from ductile materials under both proportional and out-of-phase loading cannot be accurately assessed by any of the methods from the literature, although some approaches are well suited for a safe design of welded joints. However, both methods developed in this paper, the NN and the SEC, prove to reliably provide accurate and precise fatigue life calculations for all fatigue tests in the database, including variable amplitudes. The extent of the created database allows a comprehensive evaluation of fatigue assessment approaches and the derivation of correlations between loading variables and the fatigue life. The size and diversity of the present database prevent overfitting of the developed models to specific fatigue test characteristics, which makes them robust and widely applicable.

A major advantage of the SEC is the ease of application. While providing better predictions, the SEC is easier to use and more consistent than existing approaches because of a uniform criterion with a comparison value of $CV = 1$. By adjusting only the exponents under non-proportional loading, no pre-assessment of the degree of multiaxiality as required by the GPC is needed. And unlike the FKMC, proportional and non-proportional loading can be easily accounted for without relying on different criteria. The exponents of the SEC are assumed to be the same for normal and shear stress, as there is no indication from the data that the two stress components have significantly different effects. Alternatively to optimizing the exponents for non-proportional loading, any criterion that accurately evaluates proportional loading, such as the GPC, could have been modified by optimizing a penalty factor, which is equivalent to the comparison value for the GPC. Optimizing the comparison value in the same way as for the exponents of the SEC (see Sects. 3.3 and 4.2), while keeping constant exponents of 2.0, results in a comparison value of $CV = 0.68$ (with an empirical standard deviation of 0.11) for phase shifts of both $\varphi = 90°$ and $\varphi > 0°$. An optimization based on proportional loading gives a comparison value of $CV = 1.03$ (with an empirical standard deviation of 0.10), confirming the accuracy of the GPC for proportional loading. The fatigue life assessment of both constant and variable amplitude in- and out-of-phase loading using the GPC with an optimized comparison value of $CV = 0.68$ for out-of-phase loading is presented in Appendix 4. Since the data do not include fatigue tests with a dominant stress component, the results are of similar quality as from the SEC (compare with Fig. 4). However, the issue of assessing load scenarios with a dominant stress component is not solved.

The NN learned correlations similar to the interaction equations from the SEC for proportional and out-of-phase loading, indicating that there are no significantly superior relationships between the selected input variables. Since both the SEC and the NN already predict the fatigue life of all test sets well, with a prediction quality under out-of-phase loading close to that of proportional loading (see Appendix 3), further potential dependencies do not appear to be crucial for the evaluation of proportional and out-of-phase loading. Accordingly, variables such as mean stress or R-value did not improve performance and are therefore not included.

Both the interaction equations and the NN are based on empirical correlations between loading conditions and fatigue life. The EESH is the only method capable of considering a reduction in fatigue life due to non-proportional loading based on a physical understanding rather than empirical correlations. Although non-proportional loading other than out-of-phase loading cannot be assessed by the current definition, an extension to general stress-time histories is possible because the damage parameter $F(\varphi)$ is not tied to specific loading conditions. However, the method assumes that different phase shifts have different effects on the fatigue life [32], which needs to be verified by further experiments.

Limited by the available data, all methods are evaluated under proportional and out-of-phase loading based on stresses normal to the weld and shear stresses with similar degrees of utilization. No statement can be made as to how the evaluated methods will perform under other circumstances. Accordingly, further fatigue tests under non-proportional loading other than phase shifts, loading where the utilization of one stress component is dominant, and loading including stress parallel to the weld are required for a holistic evaluation. However, [22] already show that the stress parallel to the weld can be assessed in the same way as the other stress components under proportional loading. A consideration of all three stress components extends the super ellipse criterion to the super ellipsoid criterion. Non-proportional loading other than out-of-phase loading as well as various phase shifts lower than 90° will be subject of further investigations. However, phase shifts lower than 90° have not behaved significantly differently than 90° phase shifts in this study, although the available data for lower phase shifts is too limited to derive a conclusive statement. The transformation of variable amplitudes to constant amplitude equivalents according to the IIW-recommendations with a specified Miner sum of $D_{\text{spec}} = 0.5$ is not analyzed further but yields reasonable results that are consistent with the results from constant amplitudes, although the scatter is increased, as shown in Appendices 2 and 3. The effects of different welding processes or material properties are also neglected, as the methods have proven successful for ductile welded joints made of steel, aluminum, and magnesium using arc or laser beam welding without showing apparent differences. However, a uniform definition of when a welded joint is considered ductile, i.e., when non-proportional loading reduces fatigue life, is still needed.

6 Conclusion

A comprehensive database of fatigue tests performed on welded joints demonstrating ductile material behavior under proportional and out-of-phase loading due to normal and shear stress, including constant and variable amplitudes, is created in order to evaluate multiaxial fatigue life calculation approaches for welded ductile materials. Known stress-based approaches from the literature are found to be unable to accurately predict fatigue life based on the created database, and new approaches providing reliable and accurate predictions are developed. These include the super ellipse criterion derived from the interaction equations proposed by codes and standards, as well as artificial neural networks, both developed and optimized based on the created database. A detailed analysis of the fatigue data, the interaction equations, and the neural networks reveals the correlations between multiaxial loading and fatigue life and finds the neural networks to have learned behavior similar to that represented by the super ellipse criterion. As the super ellipse criterion provides more accurate and precise calculations and is both more consistent and easier to apply than existing approaches, allowing a consistent evaluation also when one stress component is dominant, inclusion in codes and standards, such as the IIW-recommendations, is proposed.

Appendix 1 Uniaxial S-N curve parameters

Table 8 S–N curve parameters for uniaxial loading under constant amplitude loading – fixed knee point and slope after the knee point if the knee point could not be identified

Test program	Normal stress				Shear stress			
	N_{knee}	$\Delta\sigma_{knee}$	m	m*	N_{knee}	$\Delta\tau_{knee}$	m	m*
01	1e7	54.97	5.20	22.00	1e8	56.10	7.68	22.00
02	313,500	18.56	2.52	21.74	1,006,992	34.11	3.78	27.82
03	360,841	18.57	2.98	37.86	1,733,177	32.65	3.04	33.00
04	1e7	105.59	5.14	22.00	1e8	49.14	4.96	22.00
05	1e7	66.09	4.06	22.00	1e8	35.17	3.42	22.00
06	1e7	38.69	2.50	22.00	1e8	59.59	4.69	22.00
07	1e7	148.20	4.56	22.00	1e8	174.10	9.17	22.00
08	1e7	356.92	8.18	22.00	1e8	123.74	6.63	22.00
09	1e7	81.99	5.15	22.00	1e8	140.01	12.53	22.00
10	2,070,227	26.81	3.19	29.87	1e8	22.63	4.42	22.00
11	3,014,089	27.54	4.04	17.33	1e8	34.19	6.34	22.00
12	1e7	66.83	2.80	22.00	1e8	80.42	5.10	22.00
13	1e7	136.33	4.23	22.00	1e8	147.87	8.56	22.00
14	1e7	123.01	4.69	22.00	1e8	102.60	5.48	22.00

Appendix 2 Multiaxial fatigue life assessment under constant amplitude loading

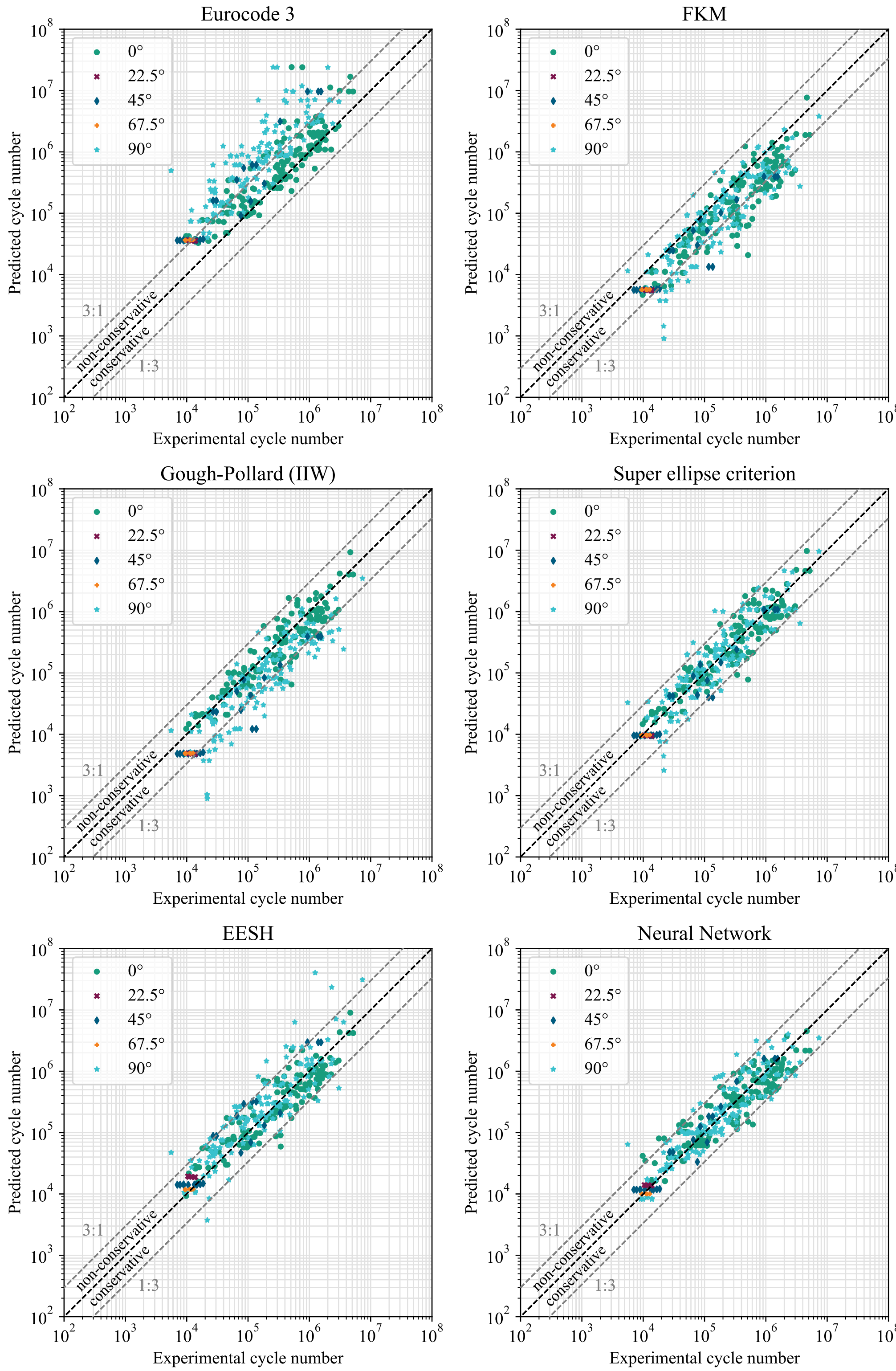

Fig. 7 Fatigue life prediction of welded joints under multiaxial loading for different phase shifts and constant amplitude loading (exemplary fatigue life prediction factors in grey)

Fig. 8 Ratio of predicted fatigue life to experimental fatigue life under constant amplitude multiaxial loading calculated by different approaches

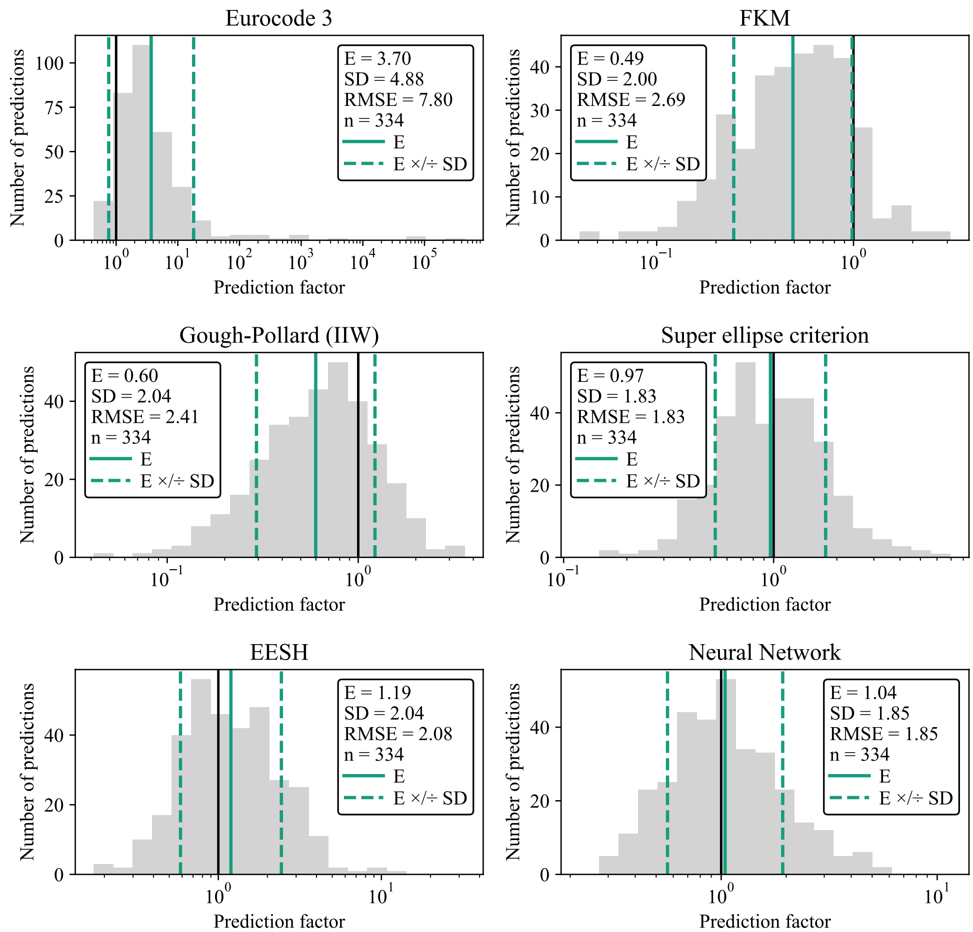

Appendix 3 Multiaxial fatigue life assessment by the super ellipse criterion

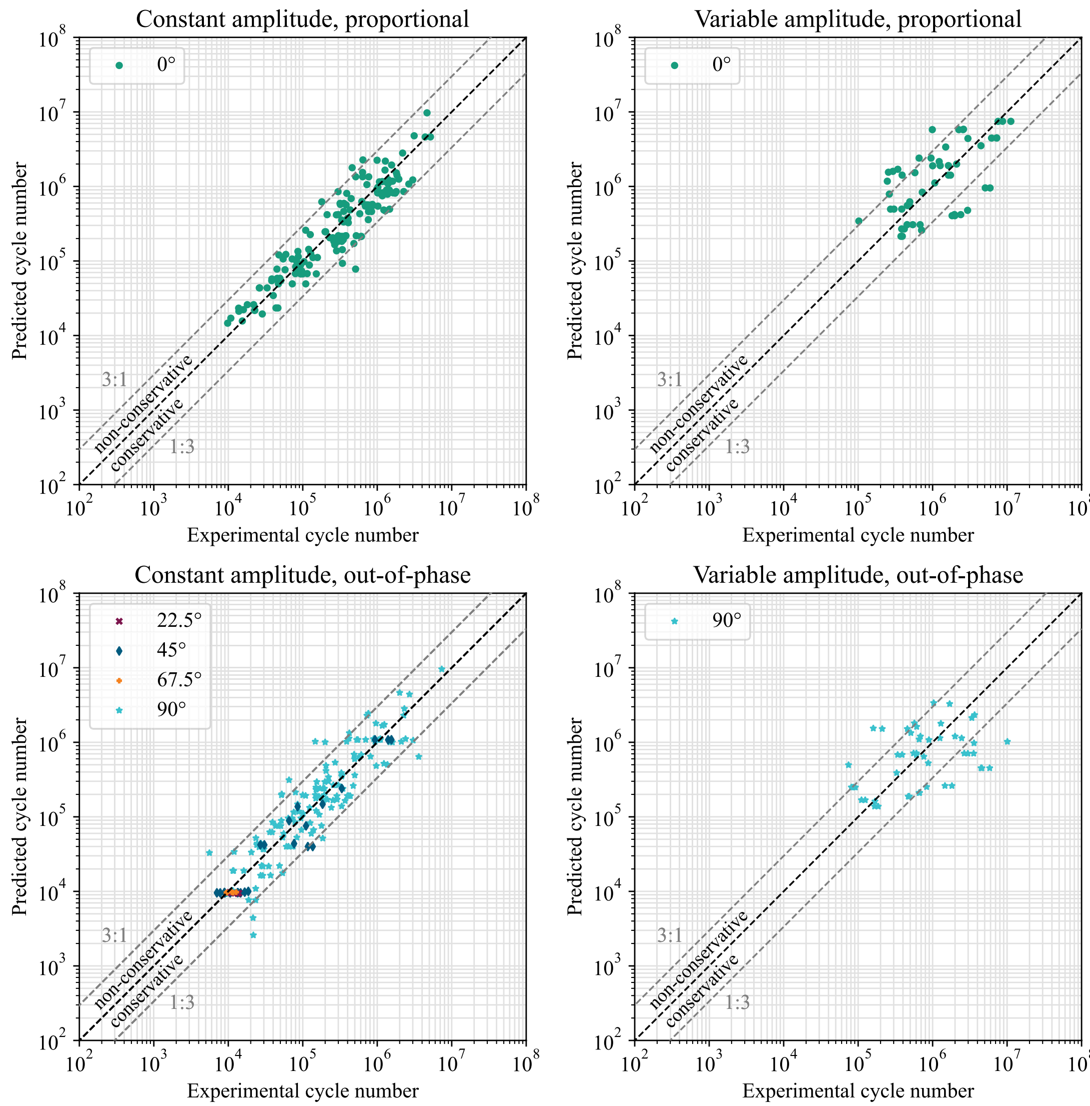

Fig. 9 Fatigue life prediction of welded joints under different loading conditions using the SEC (exemplary fatigue life prediction factors in grey)

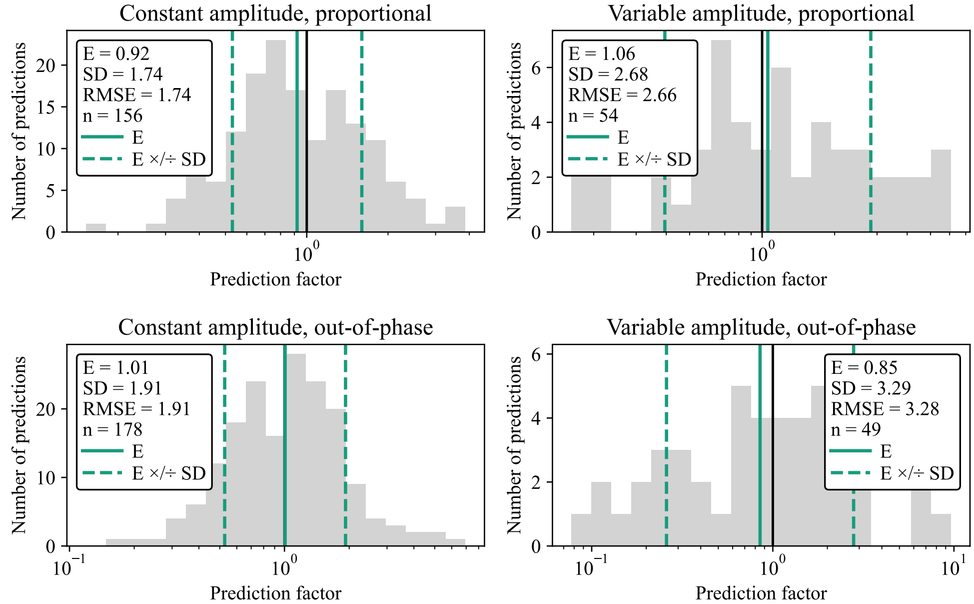

Fig. 10 Ratio of predicted fatigue life to experimental fatigue life calculated by the SEC under different loading conditions

Appendix 4 Multiaxial fatigue life assessment by the Gough-Pollard criterion based on an optimized comparison value

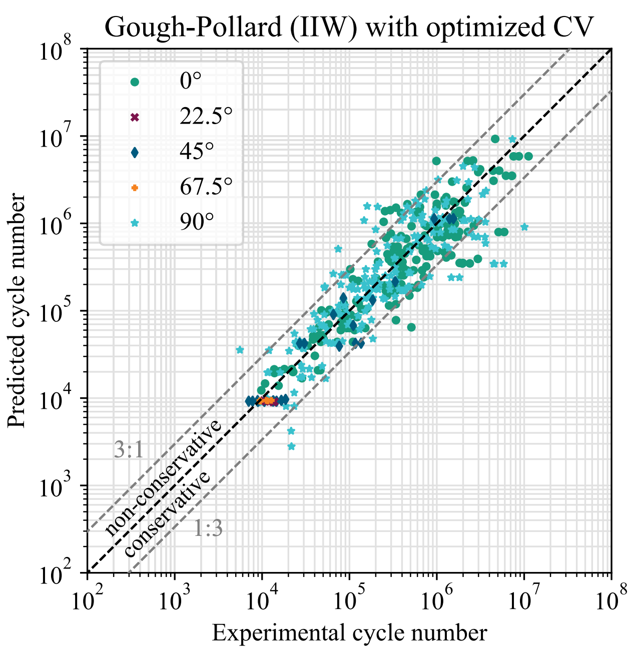

Fig. 11 Fatigue life prediction of welded joints using the GPC with $CV = 0.68$ (exemplary fatigue life prediction factors in grey)

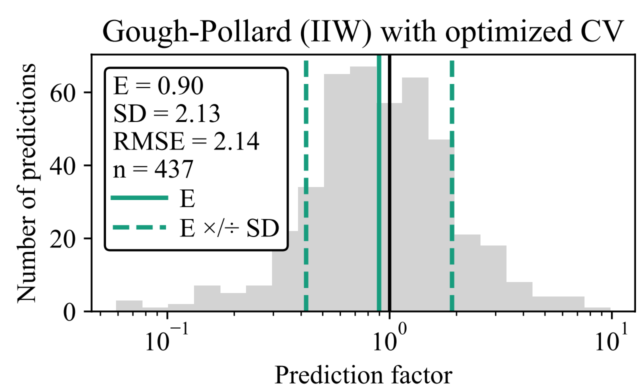

Fig. 12 Ratio of predicted fatigue life to experimental fatigue life calculated by the GPC with $CV = 0.68$

Acknowledgements The authors would like to thank the German Federal Ministry for Economic Affairs and Climate Action (BMWK) for financially supporting the research activities within the SMATRA project by a resolution of the German Bundestag.

Author contribution Niklas Michael Bauer: Conceptualization; data curation; formal analysis; investigation; methodology; project administration; software; validation; visualization; writing, original draft; writing, review and editing. Jörg Baumgartner: Conceptualization, funding acquisition, supervision, writing—review and editing.

Funding Open Access funding enabled and organized by Projekt DEAL. The research leading to these results received funding from the German Federal Ministry for Economic Affairs and Climate Action (BMWK) within the SMATRA project under Grant Agreement No. 03SX559 C.

Data availability Data will be made available upon request.

Declarations

Competing interests The authors declare no competing interests.

References

1. Sonsino CM (2011) Influence of material's ductility and local deformation mode on multiaxial fatigue response. Int J Fatigue 33(8):930–947. https://doi.org/10.1016/j.ijfatigue.2011.01.010
2. Sonsino CM (2020) Multiaxial fatigue life response depending on proportionality grade between normal and shear strains/stresses and material ductility. Int J Fatigue 135:105468. https://doi.org/10.1016/j.ijfatigue.2019.105468
3. Hobbacher AF, Baumgartner J (2024) Recommendations for fatigue design of welded joints and components, Third Edition. Springer Cham, IIW Collection.
4. EN 1993-1-9:2005+AC:2009 (2009) Eurocode 3: design of steel structures – Part 1-9: Fatigue, CEN, Brussels
5. FKM-Richtlinie (2020) Rechnerischer Festigkeitsnachweis für Maschinenbauteile, VDMA, 7th edition.
6. DNV-RP-C203 (2024) Fatigue design of offshore steel structures, DNV recommended practice.
7. Findley WN (1959) A theory for the effect of mean stress on fatigue of metals under combined torsion and axial load or bending. J Eng Industry 81(4):301–305. https://doi.org/10.1115/1.4008327
8. Matake T (1977) An explanation on fatigue limit under combined stress. Bulletin of JSME 20(141):257–263. https://doi.org/10.1299/jsme1958.20.257
9. Van Dang K, Griveau B, Message O (1989) On a new multiaxial fatigue limit criterion: Theory and application biaxial and multiaxial fatigue, EGF 3. Mechanical Engineering Publications, London, pp 479–496
10. McDiarmid DL (1985) Fatigue under out-of-phase biaxial stresses of different frequencies. In Multiaxial fatigue. ASTM International, https://doi.org/10.1520/STP36245S.
11. Susmel L (2008) Modified Wöhler curve method, theory of critical distances and Eurocode 3: a novel engineering procedure to predict the lifetime of steel welded joints subjected to both uniaxial and multiaxial fatigue loading. Int J Fatigue 30(5):888–907. https://doi.org/10.1016/j.ijfatigue.2007.06.005
12. Carpinteri A, Spagnoli A, Vantadori S (2009) Multiaxial fatigue life estimation in welded joints using the critical plane approach. Int J Fatigue 31(1):188–196. https://doi.org/10.1016/j.ijfatigue.2008.03.024
13. Kueppers M, Sonsino CM (2006) Assessment of the fatigue behaviour of welded aluminium joints under multiaxial spectrum loading by a critical plane approach. Int J Fatigue 28(5–6):540–546. https://doi.org/10.1016/j.ijfatigue.2005.07.046
14. Papadopoulos IV (1994) A new criterion of fatigue strength for out-of-phase bending and torsion of hard metals. Int J Fatigue 16(6):377–384. https://doi.org/10.1016/0142-1123(94)90449-9
15. Sonsino CM (1995) Multiaxial fatigue of welded joints under in-phase and out-of-phase local strains and stresses. Int J Fatigue 17(1):55–70. https://doi.org/10.1016/0142-1123(95)93051-3
16. Zenner H, Richter I (1977). Eine Festigkeitshypothese für die Dauerfestigkeit bei beliebigen Beanspruchungskombinationen. In: Konstruktion 29, no. 1 (1977), p. 11–18.
17. Bolchoun A (2018) Eine Methode zur Festigkeitsbeurteilung von laserstrahlgeschweißten Magnesium-Verbindungen unter mehrachsigen Beanspruchungen mit konstanten und variablen Amplituden. Dissertation, Technical University Darmstadt, https://doi.org/10.24406/publica-fhg-282368.
18. Störzel K, Wiebesiek J, Bruder T, Hanselka H (2008) Betriebsfeste Bemessung von mehrachsig belasteten Laserstrahlschweißverbindungen aus Stahlfeinblechen des Karroseriebaus. Fraunhofer-Institut für Betriebsfestigkeit und Systemzuverlässigkeit LBF, LBF-Bericht Nr. FB-235, Darmstadt, https://doi.org/10.24406/publica-fhg-298679.
19. Wiebesiek J, Störzel K, Bruder T, Kaufmann H (2011) Multiaxial fatigue behaviour of laserbeam-welded thin steel and aluminium sheets under proportional and non-proportional combined loading. Int J Fatigue 33(8):992–1005. https://doi.org/10.1016/j.ijfatigue.2010.12.008
20. Bolchoun A, Baumgartner J, Kaufmann H (2017) A new method for fatigue life evaluation under out-of-phase variable amplitude loadings and its application to thin-walled magnesium welds. Int J Fatigue 101:159–168. https://doi.org/10.1016/j.ijfatigue.2017.01.012
21. Pedersen MM (2016) Multiaxial fatigue assessment of welded joints using the notch stress approach. Int J Fatigue 83:269–279. https://doi.org/10.1016/j.ijfatigue.2015.10.021
22. Bauer NM, Baumgartner J, Fass M (2024) Fatigue life evaluation of welded joints under multiaxial loading for different stress concepts using an extended Gough-Pollard criterion. Welding in the World, 1–15, https://doi.org/10.1007/s40194-024-01716-6.
23. Sonsino CM, Baumgartner J, Breitenberger M (2022) Equivalent stress concepts for transforming of variable amplitude into constant amplitude loading and consequences for design and durability approval. Int J Fatigue 162:106949. https://doi.org/10.1016/j.ijfatigue.2022.106949
24. Sonsino CM (2009) Multiaxial fatigue assessment of welded joints–recommendations for design codes. Int J Fatigue 31(1):173–187. https://doi.org/10.1016/j.ijfatigue.2008.06.001
25. Wiebesiek J (2012) Festigkeitshypothesen zum Schwingfestigkeitsverhalten von dünnwandigen Laserstrahlschweißverbindungen aus Aluminium unter mehrachsigen Beanspruchungen mit

konstanten und veränderlichen Hauptspannungsrichtungen. Dissertation, Technical University Darmstadt.
26. Eibl M (2004) Berechnung der Schwingfestigkeit laserstrahlgeschweißter Feinbleche mit lokalen Konzepten. Dissertation, Technical University Darmstadt.
27. Exel N (2013) Schwingfestigkeit laserstrahlgeschweißter Magnesiumknetlegierungen unter mehrachsigen proportionalen und nichtproportionalen Beanspruchungen. Dissertation, Technical University Darmstadt.
28. Bertini L, Cera A, Frendo F (2014) Experimental investigation of the fatigue resistance of pipe-to-plate welded connections under bending, torsion and mixed mode loading. Int J Fatigue 68:178–185. https://doi.org/10.1016/j.ijfatigue.2014.05.005
29. Frendo F, Bertini L (2015) Fatigue resistance of pipe-to-plate welded joint under in-phase and out-of-phase combined bending and torsion. Int J Fatigue 79:46–53. https://doi.org/10.1016/j.ijfatigue.2015.04.020
30. Razmjoo GR (1997) Fatigue of load-carrying fillet welded joints under multiaxial loading. In 5 th International Conference on Biaxial/Multiaxial Fatigue & Fracture, 53–70.
31. Sonsino CM (1997) Schwingfestigkeit von geschweißten Komponenten unter komplexen elasto-plastischen, mehrachsigen Verformungen. European Commission, technische forschung stahl, report EUR 16024, Luxembourg.
32. Sonsino CM, Küppers M, Gäth N, Maddox SJ, Razmjoo GR (1999) Fatigue behaviour of welded high strength components under combined multiaxial variable amplitude loading. Fraunhofer Institute for Structural Durability and System Reliability LBF, Technical report no. LBF-FB-218.
33. Winther NB, Jensen MA, Andreasen JH, Schjødt-Thomsen J, Larsen ML (2024) Effect of non-proportional stress states caused by varying phase shifts on the fatigue life of welded joints. Int J Fatigue 185:108351. https://doi.org/10.1016/j.ijfatigue.2024.108351
34. Witt M (2000) Schwingfestigkeit von Schweißverbindungen bei zusammengesetzter Betriebsbeanspruchung. Dissertation, Technical University Clausthal.
35. Küppers M (2006) Betriebsfestigkeit von Aluminiumschweißverbindungen unter mehrachsigen Spannungszuständen mit konstanten und veränderlichen Hauptspannungsrichtungen. Dissertation, Technical University Darmstadt.
36. Pereira Baptista CA (2016) Multiaxial and variable amplitude fatigue in steel bridges. Dissertation No. 7044, Swiss Federal Institute of Technology in Lausanne and University of Lisbon, https://doi.org/10.5075/epfl-thesis-7044.
37. Garcia MAR (2020) Multiaxial fatigue analysis of high-strength steel welded joints using generalized local approaches. Dissertation No. 7394, Swiss Federal Institute of Technology in Lausanne, https://doi.org/10.5075/epfl-thesis-7394.
38. Dahle T, Olsson KE, Jonsson B (1997) High strength welded box beams subjected to torsion and bending–test results and proposed design criteria for torsion/bending interaction. In Proc. First North European Engineering and Science Conference, Welded High Strength Steel Structures, Stockholm, Sweden (pp. 143–161).
39. Archer R (1987) Fatigue of a welded steel attachment under combined direct stress and shear stress. In International conference of fatigue of welded constructions 50:62-72
40. Bäckström M, Siljander A, Kuitunen R, Ilvonen R (1997) Multiaxial fatigue experiments of square hollow section tube-to-plate welded joints. In 1st North European Engineering and Science Conference (NESCO I). Engineering Materials Advisory Services EMAS.
41. Van Lieshout PS (2020) On the assessment of multiaxial fatigue resistance of welded steel joints in marine structures when exposed to non-proportional constant amplitude loading. Dissertation Delft Univ Technol. https://doi.org/10.4233/uuid:afd39f40-7569-4cc6-ac1a-659342b45f9a
42. Khurshid M, Barsoum Z, Däuwel T, Barsoum I (2017) Root fatigue strength assessment of fillet welded tube-to-plate joints subjected to multi-axial stress state using stress based local methods. Int J Fatigue 101:209–223. https://doi.org/10.1016/j.ijfatigue.2017.02.007
43 Lotsberg I (2009) Fatigue capacity of load carrying fillet-welded connections subjected to axial and shear loading. ASME. J Offshore Mech Arct Eng 131(4):041302. https://doi.org/10.1115/1.3160531
44. Fricke W, Robert C, Peters R, Sumpf A (2016) Fatigue strength of laser-stake welded T-joints subjected to combined axial and shear loads. Weld World 60:593–604. https://doi.org/10.1007/s40194-016-0322-z
45. Yung JY, Lawrence FV Jr (1989) Predicting the fatigue life of welds under combined bending and torsion. Mechanical Engineering Publications, Biaxial and Multiaxial Fatigue, pp 53–69
46. Bokesjö M, Al-Emrani M, Svensson T (2012) Fatigue strength of fillet welds subjected to multi-axial stresses. Int J Fatigue 44:21–31. https://doi.org/10.1016/j.ijfatigue.2012.06.004
47. Khurshid M, Barsoum Z, Barsoum I et al (2016) The multiaxial weld root fatigue of butt welded joints subjected to uniaxial loading. Fatigue Fract Eng Mater Struct 39(10):1281–1298. https://doi.org/10.1111/ffe.12444
48. Shen W, Yan R, Liu E et al (2015) Fatigue growth behavior for surface crack in welding joints under combined compressive and bending stresses. Int J Fatigue 77:50–63. https://doi.org/10.1016/j.ijfatigue.2015.03.005
49. Wagner M, Faß M (2022) Schwingfeste Auslegung laserstrahlgeschweißter Verbindungen unter mehrachsiger Beanspruchung (Engl.: Fatigue resistant design of laser beam welded joints under multiaxial loading). Final report. IGF-Project 20621 BG / 2.
50. Siljander OA (1991) Nonproportional biaxial fatigue of welded joints. Dissertation, University of Illinois at Urbana-Champaign.
51. Takahashi I, Takada A, Ushijima M et al (2003) Fatigue behaviour of a box-welded joint under biaxial cyclic loading: effects of biaxial load range ratio and cyclic compressive loads in the lateral direction. Fatigue Fract Eng Mater Struct 26(5):439–448. https://doi.org/10.1046/j.1460-2695.2003.00645.x
52. Pascual FG, Meeker WQ (1999) Estimating fatigue curves with the random fatigue-limit model. Technometrics 41(4):277–289. https://doi.org/10.1080/00401706.1999.10485925
53. Baumgartner J, Bruder T (2013) An efficient meshing approach for the calculation of notch stresses. Weld World 57:137–145. https://doi.org/10.1007/s40194-012-0005-3
54. Sonsino CM, Kueppers M, Eibl M, Zhang G (2006) Fatigue strength of laser beam welded thin steel structures under multiaxial loading. Int J Fatigue 28(5–6):657–662. https://doi.org/10.1016/j.ijfatigue.2005.09.013